View Article Online
View Journal

Dalton Transactions

An international journal of inorganic chemistry

Accepted Manuscript

This article can be cited before page numbers have been issued, to do this please use: Q. Mu, H. Li, R. Pang, D. Li, S. Zhang, X. Li and L. Jiang, *Dalton Trans.*, 2026, DOI: 10.1039/D5DT02917A.

ROYAL SOCIETY OF CHEMISTRY

rsc.li/dalton

View Article Online
DOI: 10.1039/D5DT02917A

Luminescence characteristics and low temperature optical temperature measurement of Pr^{3+} doped $Sr_2NaMg_2V_3O_{12}$ phosphors

Qiuyue Mu [a,b], Huimin Li [b], Ran Pang [b], Da Li [b], Su Zhang [b], Xiaodong Li [a,*], Lihong Jiang [b,*]

a School of Materials Science and Engineering, Jilin Jianzhu University, Changchun, 130118, China

b China-Belarus Belt and Road Joint Laboratory on Advanced Materials and Manufacturing, Changchun Institute of Applied Chemistry, Chinese Academy of Sciences, Changchun, 130022, China

Abstract: A series of Pr^{3+} doped $Sr_2NaMg_2V_3O_{12}$ (SNMV) garnet phosphors were successfully synthesized by high temperature solid state method. The crystal structure, luminescent properties and temperature sensing properties of the phosphors were systematically studied. Under the excitation of 339 nm, SNMV:Pr^{3+} phosphors exhibit strong blue-green broadband emission in the wavelength range of 400-700 nm and typical red emission of Pr^{3+} at 612 nm and 624 nm, which correspond to the energy level transition of $[VO_4]^{3-}$ group and $^1D_2 \rightarrow {}^3H_{4,5}$ transition of Pr^{3+}, respectively. Furthermore, in the temperature range of 98-298 K, high sensitivity optical temperature sensing is realized based on fluorescence intensity ratio (FIR) and fluorescence lifetime (FL). In FIR mode, the maximum absolute sensitivity (S_a) and relative sensitivity (S_r) of the phosphor are 0.01782 K^{-1} (298 K) and 1.13543% K^{-1} (298 K), respectively. In FL mode, the maximum S_a value and S_r value are 0.0889 K^{-1} (198 K) and 0.62752% K^{-1} (223 K), respectively. The results show that SNMV:Pr^{3+} phosphors have great potential in the field of optical temperature measurement.

Key words: Pr^{3+}, garnet structure, fluorescence intensity ratio, fluorescence lifetime, optical temperature measurement

1. Introduction

In recent years, non-contact optical temperature sensing technology has shown broad application prospects in the fields of intelligent manufacturing, biomedicine, new energy and extreme environmental monitoring. This technology has the

View Article Online
DOI: 10.1039/D5DT02917A

advantages of high sensitivity and precision, high spatial resolution, fast dynamic response and strong anti-interference ability, especially suitable for accurate temperature measurement in nanometer scale or extreme environment[1-3]. The fluorescence temperature measurement method based on rare earth doped fluorescent materials is a research hotspot at present. At present, the commonly used fluorescence temperature measurement strategies include fluorescence intensity ratio method, fluorescence lifetime temperature measurement method, fluorescence spectrum peak shift method and so on. Among them, the fluorescence intensity ratio method (FIR) is one of the most commonly used fluorescence temperature measurement strategies at present. The principle is to measure the temperature by using the dependence of the emission intensity ratio of fluorescent materials at different wavelengths on temperature. This method has strong anti-interference ability[4-6]. In addition, fluorescence lifetime thermometry is another commonly used and effective temperature measurement strategy with high accuracy, which can avoid the interference of stimulated luminescence intensity, fluorescence quenching and other factors. Two different temperature measurement strategies, FIR and FL, are used for fluorescence temperature measurement, which helps to reduce the influence of environmental factors and material properties, so as to improve the temperature measurement accuracy, enhance the anti-interference ability and broaden the application range[7-11].

Finding two emission peaks with different thermal responses is the key to constructing FIR temperature measurement. Usually, FIR temperature measurement uses two thermally coupled levels (TCLs). However, this method requires the energy range difference (ΔE) of the two emission levels to be between 200-2000 cm^{-1}, which greatly limits the improvement of temperature measurement sensitivity[12]. In order to solve this problem, two different luminescence centers are used to measure the temperature according to the non thermally coupled energy levels (NTCLs), which can effectively improve the temperature measurement sensitivity[13]. Vanadate materials have large band gap, low phonon energy and excellent chemical stability. As the luminescence center, $[VO_4]^{3-}$ can produce strong broadband emission in the visible region due to the charge transfer transition from ligand O^{2-} to metal V^{5+} [14]. In vanadate system, garnet structure provides more options for adjusting emission and sensing properties by virtue of its unique structural framework and flexible cation substitution[15]. Among rare earth ions, Pr^{3+} has become an attractive activating ion due

View Article Online
DOI: 10.1039/D5DT02917A

to its luminescence in the UV, visible and near-infrared ranges. Its luminescence generally comes from transitions in $^3P_{0,1}$ and $^1D_2$ multiple states. In previous studies, Pr^{3+} doped phosphors also showed excellent temperature measurement ability[4,16-18]. For example, Mouna Fhoula et al. used FIR technology to study the temperature dependent luminescence behavior of TCLs and NTCLs of Pr^{3+}/Yb^{3+} codoped $Y_2Mo_4O_{15}$ phosphor at 298-508 K[4]. N. Navya et al reported a new red luminescent material $CeO_2:Pr^{3+}$ prepared by green combustion method, with a relative sensitivity of 2.65% K^{-1} and an absolute sensitivity of 0.023 K^{-1} in the temperature range of 303-603 K[16]. Anu et al. established four FIR models according to the relationship between different emission peaks to explore the temperature sensitivity of $Li_2Ba_5W_3O_{15}:Pr^{3+}$ sample at 303-423 K[17]. Zheng et al. found that the presence of Pr^{3+} ions and the $4d^0$ electronic configuration of W^{6+} in the host can lead to the formation of IVCT state and interfere with the emission of 4f energy level of rare earth ions, thus exploring the optical temperature sensing characteristics of $SrWO_4:Pr^{3+}$ material at 298-598 K[18]. However, there are few studies on the temperature sensing properties of Pr^{3+} doped phosphors in the low temperature range of 98-298 K. In order to make up for this deficiency, a $Sr_{2-2x}Na_{1+x}Mg_2V_3O_{12}:xPr^{3+}$ phosphor system was proposed in this work. Under UV excitation, $[VO_4]^{3-}$ and Pr^{3+} as two different luminescence centers show different temperature responses, which can realize FIR temperature measurement based on NTCLs.

In this paper, the crystal structure of Pr^{3+} doped $Sr_2NaMg_2V_3O_{12}$ phosphor, the photoluminescence properties at different concentrations at room temperature and the energy transfer mechanism of $[VO_4]^{3-}$ and Pr^{3+} were studied. In addition, the temperature sensing performance of phosphors was explored by using two temperature measurement techniques, namely, fluorescence intensity ratio and fluorescence lifetime, in the temperature range of 98-298 K. This work enriches the temperature sensing material library in the low temperature region, and has reference significance for the development of new non-contact fluorescent temperature measurement probe.

2. Experimental part and characterization

Sample preparation

SNMV:Pr^{3+} phosphors were prepared by high temperature solid state method. The raw materials in the experiment were $SrCO_3$ (West Asia reagent, 99.5%), Na_2CO_3

View Article Online
DOI: 10.1039/D5DT02917A

(Aladdin, GR ≥ 99.8%), $(MgCO_3)_4$•$Mg(OH)_2$ (West Asia reagent, 99%), NH_4VO_3 (Xilong, AR), Pr_6O_{11} (Jinan Henghua, 99.99%). First, mix the raw materials in stoichiometric proportion and grind them in an agate mortar for 30 minutes. Then, the milled sample is transferred to the alumina crucible and calcined in the muffle furnace at 600 ℃ air atmosphere for 2 h. After cooling to room temperature, the sample is taken out for full grinding. Then, it was calcined at 900 ℃ for 6 h in an air atmosphere in a muffle furnace. After cooling to room temperature, it was taken out and fully ground in an agate mortar to prepare the required samples.

Performance characterization

The crystal structure of the sample was measured by Bruker D8 X-ray diffractometer (German Bruker AXS company) with Cukα radiation source (λ = 1.5406 Å). The scanning range was 2θ = 10-90 °, the scanning speed was 10 °/min, the working current was 40 mA, and the working voltage was 40 kV. The surface morphology and element images of the samples were characterized by Hitachi S-4800 field emission scanning electron microscope (SEM). Using the FLS920 (Edinburgh instruments) high-resolution fluorescence spectrometer equipped with 450 W continuous wavelength xenon (Xe) lamp as the light source and Shimadzu R9287 (Hamamatsu K.K) photomultiplier tube (200-900 nm) as the detector, the temperature change spectrum and fluorescence lifetime of the samples were obtained.

3. Results and discussion

3.1 Phase analysis

View Article Online
DOI: 10.1039/D5DT02917A

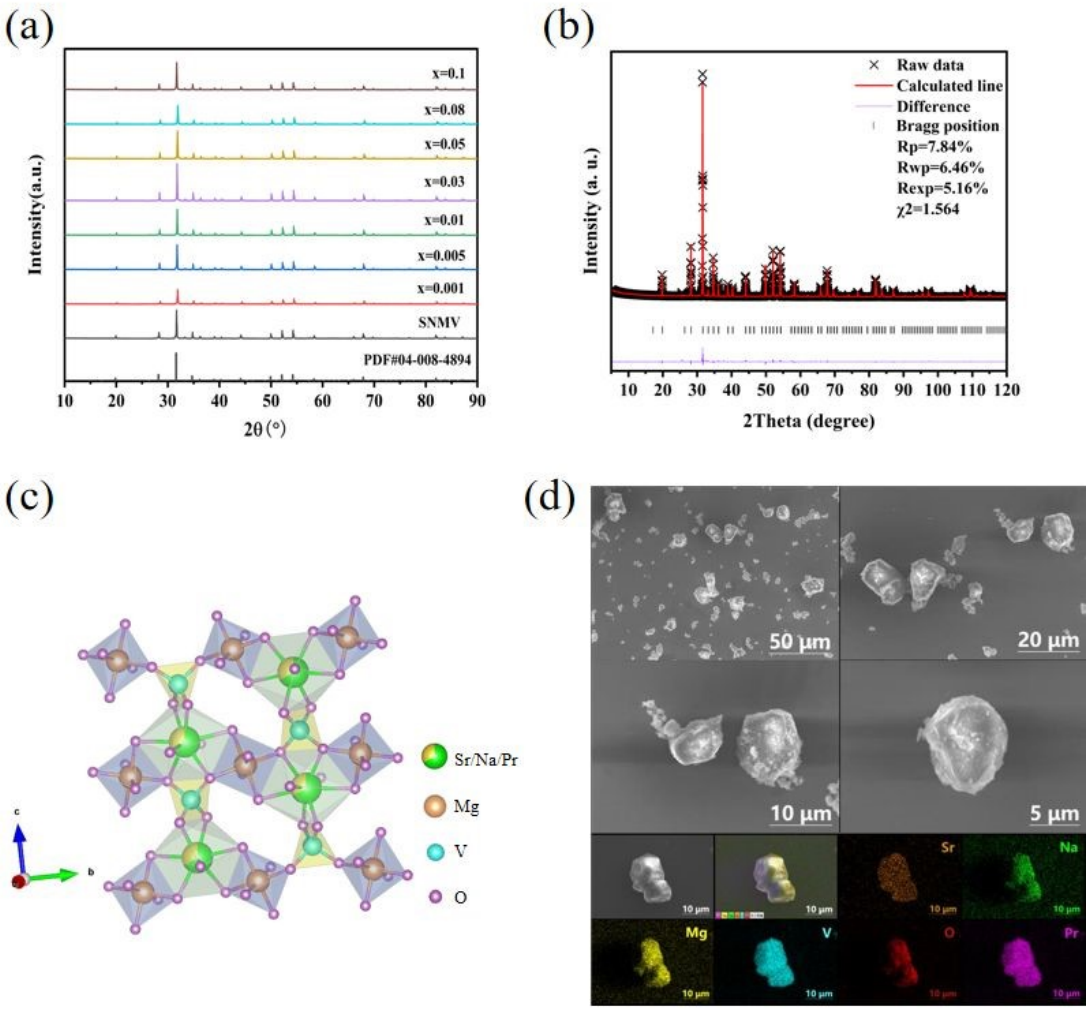

Fig.1 (a) XRD patterns of $Sr_{2-2x}Na_{1+x}Mg_2V_3O_{12}$:x$Pr^{3+}$ (x=0.001-0.1) phosphor and the standard card of SNMV; (b) XRD Rietveld refined spectrum of SNMV:0.03Pr^{3+} phosphor; (c) The crystal structure of SNMV:0.03Pr^{3+} phosphor; (d) SEM and elemental distribution of SNMV:0.03Pr^{3+} phosphor.

Fig.1 (a) shows the XRD patterns of the prepared SNMV host and samples doped with different concentrations of Pr^{3+}. It can be seen from the figure that the diffraction peak of the host is consistent with the standard card PDF#04-008-4894, indicating that the single-phase SNMV powder was successfully synthesized. There is no impurity peak after doping with different concentrations of Pr^{3+}, indicating that Pr^{3+} is successfully doped into the lattice. Fig.1 (b) shows the XRD data of SNMV:0.03Pr^{3+} phosphor and its Rietveld structure refinement results. The "X" in the figure is the powder diffraction data, the red solid line is the calculation curve

View Article Online
DOI: 10.1039/D5DT02917A

obtained by fitting, the purple solid line represents the difference between the two, and the black vertical line below represents the lattice position. The fitting results show that the calculated spectral lines are in good agreement with the experimental data, and the refined factor values are *Rp*=7.84%, *Rwp*=6.46%, χ^2=1.564, respectively. The lower values of *Rp* and *Rwp* show that the error is small, so the refined results can be considered to be reliable. Table 1 shows the corresponding lattice parameters and cell volume of SNMV:0.03Pr^{3+} powder.

The crystal structure model of SNMV:0.03Pr^{3+} is shown in Fig.1 (c). The compound belongs to cubic crystal system with space group Ia-3d (230) and garnet structure. The cell parameters are $a = b = c$ =12.65869 Å, α = 90 °, V = 2028.459 $Å^3$. Table 2 shows the atomic coordinates of the sample. The whole crystal structure is composed of three different coordination polyhedrons, including [Sr/Na/PrO_8], [MgO_6] and [VO_4] groups, which are bridged by oxygen atoms to form a stable three-dimensional skeleton. In these crystal lattices, the [Sr/NaO_8] polyhedron is an irregular eight coordination structure, and Sr and Na occupy this lattice together. [MgO_6] polyhedron is a typical octahedral structure. Mg atoms coordinate with six O atoms to form a regular octahedral structure. The [VO_4] group has a tetrahedral structure, in which *V* is stable in the form of tetra coordination. It is an important center for energy absorption and transfer in garnet structure[16-18]. From the perspective of ion radius, we speculate that Pr^{3+} (1.126 Å, CN = 8) occupies the Sr, Na sites. The acceptable radius relative difference (*Dr*) between doped ions and host ions is less than 30%[19,20], and the calculation formula is:

$$Dr = 100\% \times \frac{R_{m(CN)} - R_{d(CN)}}{R_{m(CN)}} \quad (1)$$

Where R_m and R_d represent the radii of substituted host ions and doped ions respectively, and CN is the coordination number. Table 3 lists the Dr values between the host cations and Pr^{3+}. The *Dr* values between Sr^{2+} (8), Na^+ (8), Mg^{2+} (6) and Pr^{3+} are 10.63%, 4.58% and -37.50%, respectively, which are in line with the above theory.

Table 1 Rietveld fitting results of SNMV:0.03Pr^{3+}

Formula	SNMV:0.03Pr^{3+}
Crystal system	Cubic
Spatial structure	Ia-3d

View Article Online
DOI: 10.1039/D5DT02917A

Z	8
a=*b*=*c*	12.65869
$\alpha = \beta = \gamma$	90
V	2028.459
Rp (%)	7.84
Rwp (%)	6.46
Rexp (%)	5.16
χ^2	1.564

Table 2 Atomic coordinates of SNMV:0.03Pr^{3+}

Atom	X	Y	Z	Fraction
Sr	0.125	0	0.25	0.650
Na	0.125	0	0.25	0.340
Pr	0.125	0	0.25	0.010
Mg	0	0	0	1.000
V	0.375	0	0.25	1.000
O	0.0987	0.2048	0.2882	1.000

Table 3 Relative difference value of ion radius (*Dr*) between host cation and Pr^{3+}

host cation (CN)	doped ion (CN)	R_m (Å)	R_d (Å)	*Dr* (%)
Sr^{2+} (8)	Pr^{3+} (8)	1.26	1.126	10.63
Na^{+} (8)	Pr^{3+} (8)	1.18	1.126	4.58
Mg^{2+} (6)	Pr^{3+} (6)	0.72	0.99	-37.50

Fig.1 (d) shows the SEM image and element distribution of SNMV:0.03Pr^{3+} phosphor. It can be seen from the SEM image that the phosphor is composed of irregular particles. With the increase of magnification, it can be clearly observed that the particles are irregular polyhedron, with clear edges, and some particles are slightly rough on the surface. The particle size is mainly concentrated in the range of 5-20 μm. The element distribution diagram shows that the constituent elements of the host

View Article Online
DOI: 10.1039/D5DT02917A

structure and doped elements are uniformly and continuously distributed in the particles. The results show that the effect of Pr^{3+} doping is good.

3.2 Luminescence properties of SNMV:Pr^{3+}

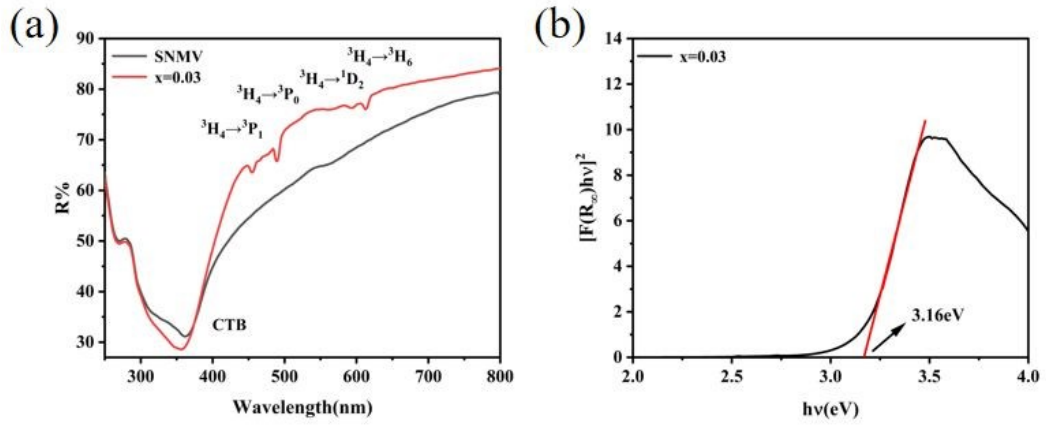

Fig.2 (a) UV-Vis diffuse reflectance spectra of SNMV:0.03Pr^{3+} (x = 0, 0.03) phosphor; (b) Curve of $\left[F\left(R_\infty\right)h\nu\right]^2$ pairs of photon energy ($h\nu$) of SNMV:0.03Pr^{3+} phosphor.

Fig.2 (a) shows the UV-Vis diffuse reflectance spectra of the host and SNMV:0.03Pr^{3+} phosphor. It can be seen from the figure that there is a strong absorption band in the 300-400 nm range of the phosphor, which is mainly due to the charge transfer band (CTB) absorption of the $[VO_4]^{3-}$ group in the host. In addition, the absorption peak in the range of 450-620 nm comes from the 4f-4f transition of Pr^{3+}. The absorption peaks at 454 nm, 488 nm, 595 nm and 612 nm come from $^3H_4 \rightarrow {}^3P_1$, $^3H_4 \rightarrow {}^3p_0$, $^3H_4 \rightarrow {}^1D_2$ and $^3H_4 \rightarrow {}^3H_6$ transitions, respectively. The curve of $\left[F\left(R_\infty\right)h\nu\right]^2$ pairs of photon energy ($h\nu$) of SNMV:0.03Pr^{3+} phosphor is shown in Fig.2 (b). Using Kubelka Munk (K-M) function and tauc formula[21], the direct optical band gap (E_g) can be obtained from $\left[F\left(R_\infty\right)h\nu\right]^2$ pairs of $h\nu$ curves:

$$R_\infty = \frac{R_{sample}}{R_{standard}} \tag{2}$$

$$F\left(R_\infty\right) = \frac{\left(1-R_\infty\right)^2}{2R_\infty} = \frac{K}{S} \tag{3}$$

$$\left[F\left(R_\infty\right)h\nu\right]^2 = A\left(h\nu - E_g\right) \tag{4}$$

Where R_∞ is the reflectance ratio of the phosphor to the ideal reference sample, $F\left(R_\infty\right)$ is the K-M function, K is the absorption coefficient, S is the scattering

View Article Online
DOI: 10.1039/D5DT02917A

coefficient, hv is the photon energy, E_g is the optical band gap value, and A is the absorption constant. The band gap width of SNMV is 3.11 eV, and that of SNMV:0.03Pr^{3+} is 3.16 eV. This increase in band gap width can be attributed to the local lattice distortion caused by the substitution of corresponding cation sites after Pr^{3+} doping[22].

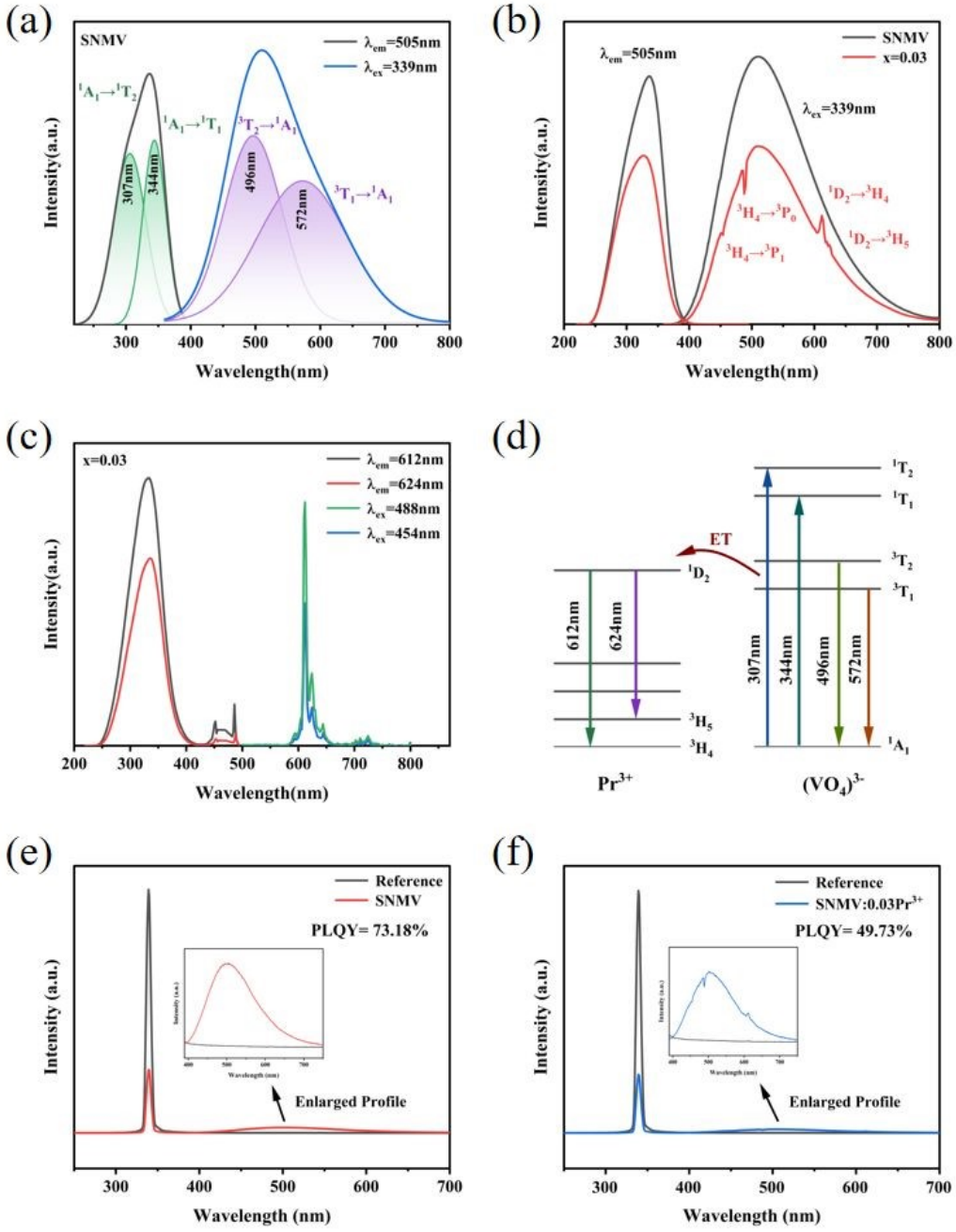

Fig.3 (a) Gaussian curves fitting of excitation and emission spectra of SNMV host; (b) Excitation spectra monitored at 505 nm and emission spectra excited at 339 nm of

View Article Online
DOI: 10.1039/D5DT02917A

SNMV host and SNMV:0.03Pr^{3+} phosphor; (c) Excitation spectra monitored at 612 nm, 624 nm and emission spectra excited at 454 nm, 488 nm of SNMV:0.03Pr^{3+} phosphor; (d) The energy transfer process of SNMV:0.03Pr^{3+} phosphor; (e) The PLQY of SNMV with 339 nm excitation; (f) The PLQY of SNMV:0.03Pr^{3+} with 339 nm excitation.

The photoluminescence spectra of SNMV are shown in Fig.3 (a). The excitation and emission spectra are asymmetric broadband emission, with excitation spectrum wavelength range of 250-400 nm, peak value of 339 nm, emission spectrum wavelength range of 400-700 nm, peak value of 505 nm. The excitation and emission spectra of the host SNMV are deconvoluted using Gaussian function, as shown in Fig.3 (a). It appears that the excitation spectrum of SNMV can be fitted by two curves located at 307 nm and 344 nm, which attributed to the $^1A_1 \rightarrow {}^1T_2$ and $^1A_1 \rightarrow {}^1T_1$ transitions of $[VO_4]^{3-}$. The emission spectrum can also be fitted by two curves located at 496 nm and 572 nm, which attributed to the $^3T_2 \rightarrow {}^1A_1$ and $^3T_1 \rightarrow {}^1A_1$ transitions of $[VO_4]^{3-}$. Fig.3 (b) shows the photoluminescence spectra of SNMV and SNMV:0.03Pr^{3+} phosphors. We found that compared with SNMV, SNMV:0.03Pr^{3+} Phosphor generated two sharp emission peaks at 612 nm and 624 nm, corresponding to $^1D_2 \rightarrow {}^3H_4$ and $^1D_2 \rightarrow {}^3H_5$ transitions of Pr^{3+}, respectively. In addition, two downward peaks at 454 nm and 488 nm can be observed, which are consistent with the characteristic absorption peaks corresponding to the $^3H_4 \rightarrow {}^3P_1$ and $^3H_4 \rightarrow {}^3P_0$ transitions of Pr^{3+}, so we speculate that the two downward peaks are caused by the overlapping of the absorption peaks of Pr^{3+} and the emission spectra of SNMV. To prove this, we tested and monitored the excitation spectra of SNMV:0.03Pr^{3+} phosphors at 612 nm and 624 nm, and the emission spectra of SNMV:0.03Pr^{3+} phosphors excited at 454 nm and 488 nm, as shown in Fig.3 (c). The characteristic excitation peaks of Pr^{3+} at 454 nm and 488 nm can be observed by monitoring the excitation spectra at 612 nm and 624 nm. The excitation spectrum of Pr^{3+} overlaps with the emission spectrum of SNMV, indicating that there is an energy transfer process between the host and Pr^{3+}. The two downward peaks at 454 nm and 488 nm in Fig.3 (b) above prove that Pr^{3+} absorbs the energy of the host.

On this basis, the energy transfer process between $[VO_4]^{3-}$ group and Pr^{3+} was studied, as shown in Fig.3 (d). Under the excitation of 339 nm, the valence band electron

View Article Online
DOI: 10.1039/D5DT02917A

absorption energy of $[VO_4]^{3-}$ group transitions from the ground state $^1A_1$ to the two higher excited states $^1T_{1,2}$, and then relaxes to the lower excited state $^3T_{1,2}$ through the non radiative transition, finally returns to the ground state and emits blue-green (400-700 nm) light. When Pr^{3+} enters the lattice, because the $^1D_2$ energy level of Pr^{3+} is similar to the $^3T_2$ and $^3T_1$ energy levels of $[VO_4]^{3-}$, the energy of the partially excited state of $[VO_4]^{3-}$ is transferred to Pr^{3+}, making the ground state electron of Pr^{3+} transition to $^1D_2$ energy level, and then from $^1D_2$ energy level to $^3H_{4,5}$ energy level, resulting in the characteristic 4f-4f transition emission of Pr^{3+} at 612 nm and 624 nm[23-25]. The PLQY of the phosphors at maximum luminescence intensity is shown in Fig.3 (e) (f), with 339 nm set as the excitation wavelength, the PLQY of SNMV is 73.18%, the PLQY of SNMV:0.03Pr^{3+} is 49.73%.

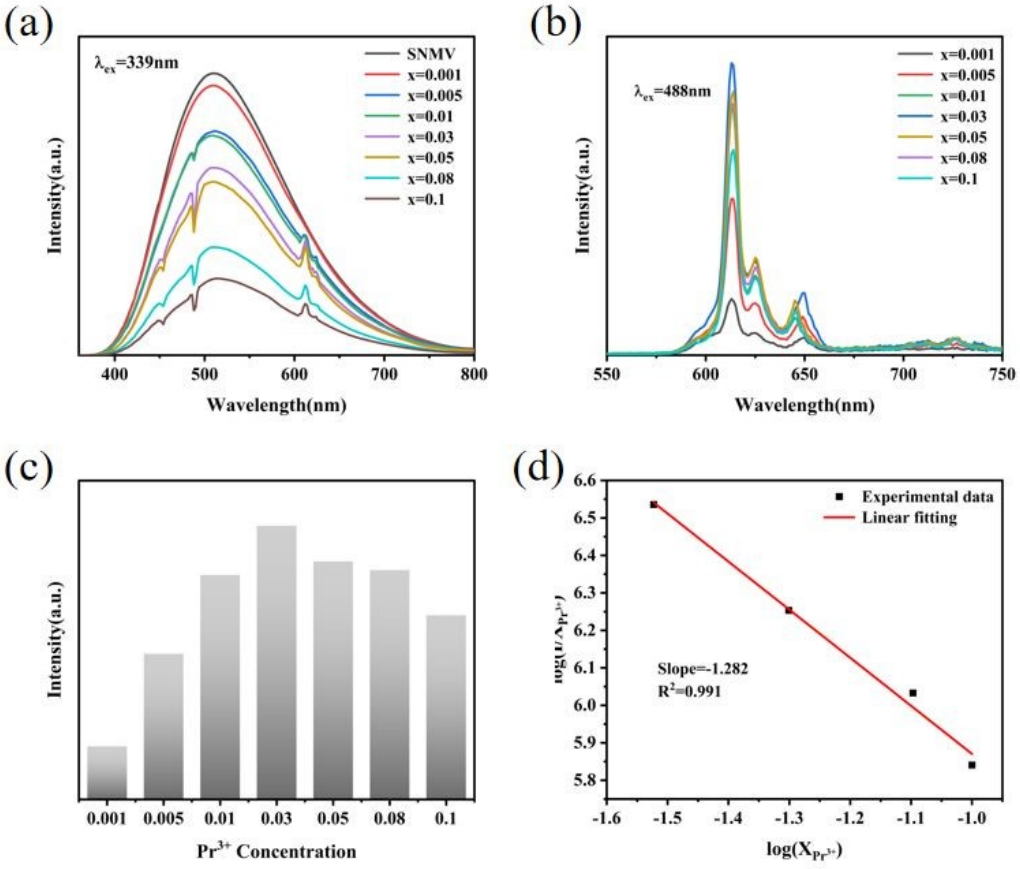

Fig.4 (a) Emission spectra of SNMV:xPr^{3+} phosphor excited at 339 nm; (b) Emission spectra of SNMV:xPr^{3+} phosphor excited at 488 nm; (c) Emission intensity comparison diagram of SNMV:xPr^{3+} phosphor; (d) The linear fitting plot of log(I/x) versus log(x) for the SNMV:xPr^{3+} (x > 0.03).

The emission spectra of SNMV:xPr^{3+} phosphor excited at 339 nm and 488 nm at

View Article Online
DOI: 10.1039/D5DT02917A

room temperature are shown in Fig.4 (a) (b). With the increase of Pr^{3+} concentration, the intensity of the emission peak at 505 nm gradually decreased, and the intensity of the emission peak at 612 nm first increased and then decreased. As can be seen from Fig.4 (c), when the concentration of Pr^{3+} is 0.03, the intensity of the emission peak at 612 nm is the strongest. The results showed that the energy transfer efficiency of $VO_4^{3-} \rightarrow Pr^{3+}$ gradually increased in the low concentration region, resulting in the decrease of self luminescence of the host and the enhancement of Pr^{3+} related luminescence. With the increase of doping concentration, the distance between Pr^{3+} decreases, and the non radiative processes such as cross relaxation become stronger, leading to the concentration quenching effect. The critical distance (R_c) between Pr^{3+} at concentration quenching was calculated by the formula[26,27]:

$$R_c \approx 2\left[\frac{3V}{4\pi X_c Z}\right]^{1/3} \quad (5)$$

Where V is the unit cell volume, X_c is the critical concentration, and Z is the coordination number. X_c is 0.03, and the critical distance R_c of Pr^{3+}-Pr^{3+} in SNMV is about 25.26 Å. Since R_c is much larger than 5 Å, exchange interaction is excluded. Therefore, the electric multipole interaction is the most likely reason for the quenching of Pr^{3+} in SNMV[28]. The specific types of electric multipole interactions between Pr^{3+} can be determined by using the formula[28,29]:

$$\frac{I}{x} = \left[1 + \beta(x)^{\theta/3}\right]^{-1} \quad (6)$$

Where I is the emission intensity, x is the Pr^{3+} concentration, β is the constant, and θ is the electrical multipole characteristic. The θ values are 6, 8 and 10, which are attributed to the electric dipole-dipole, dipole-quadrupole and quadrupole-quadrupole interaction, respectively[27]. The linear fitting plot of $\log(I/x)$ versus $\log(x)$ for the SNMV:xPr^{3+} (x > 0.03) is shown in Fig.4 (d), with a slope of -1.282 = $-\theta/3$ and a value of θ of 3.846, close to 6. Therefore, the quenching type of Pr^{3+} in SNMV is most likely electric dipole-dipole interaction.

3.3 Optical temperature measurement characteristics

View Article Online
DOI: 10.1039/D5DT02917A

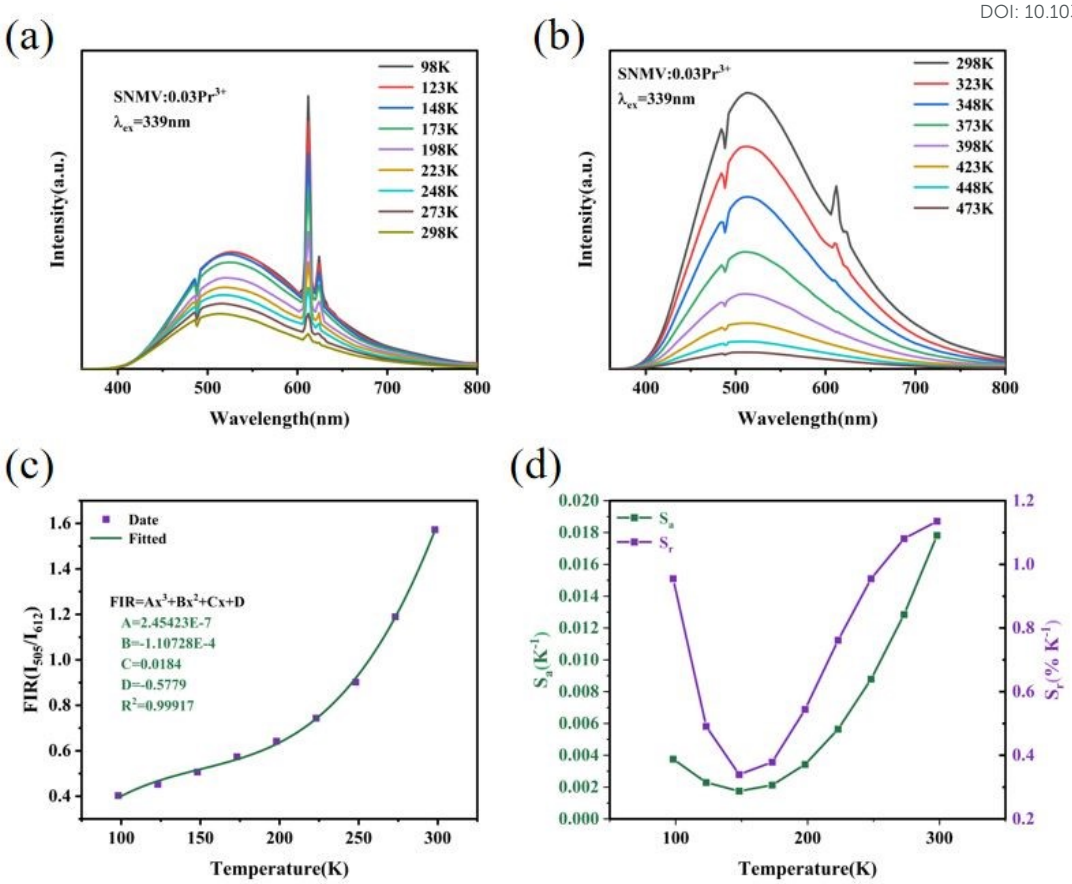

Fig.5 (a) Temperature dependent emission spectrum of SNMV:0.03Pr^{3+} phosphor in the range of 98-298 K; (b) Temperature dependent emission spectra of SNMV:0.03Pr^{3+} Phosphor in the range of 298-473 K; (c) The temperature dependence of FIR (I_{505}/I_{612}) of SNMV:0.03Pr^{3+} phosphor; (d) Absolute sensitivity S_a and relative sensitivity S_r versus temperature.

Fig.5 (a) (b) shows the temperature dependent emission spectra of SNMV:0.03Pr^{3+} phosphor in the range of 98-473 K, and its excitation wavelength is fixed at 339 nm. The low temperature (98-298 K) emission spectrum of phosphor is shown in Fig.5 (a). It can be seen from the figure that with the decrease of temperature, the overall emission intensity gradually increases, especially the emission peaks at 612 nm and 624 nm, which belong to $^1D_2 \rightarrow {}^3H_4$ and $^1D_2 \rightarrow {}^3H_5$ transitions of Pr^{3+} respectively, and are 4f-4f forbidden transitions of Pr^{3+}, and the energy mainly comes from the energy transfer of $[VO_4]^{3-}$ group. As the temperature decreases, the non radiative relaxation process that causes VO_4^{3-} to consume energy is suppressed. The energy of the excited state can be more likely to be released through two relaxation pathways: radiative luminescence or energy transfer to Pr^{3+}. Therefore,

View Article Online
DOI: 10.1039/D5DT02917A

the decrease in temperature leads to an increase in host emission, while the energy transfer efficiency of $VO_4^{3-} \rightarrow Pr^{3+}$ is improved. At 612 nm, when the temperature drops to 248 K, the luminescence intensity of $^1D_2 \rightarrow {}^3H_4$ transition from Pr^{3+} is greater than that of the host. When the temperature is 98 K, the overall luminous intensity is the strongest, and the energy transfer efficiency of $VO_4^{3-} \rightarrow Pr^{3+}$ is the highest. Fig.5 (b) shows the high temperature (298-473 K) emission spectrum of phosphor. It can be observed from the figure that the emission intensity of the sample decreases significantly with the increase of temperature. The intensity decreases to 6% of the intensity at 298 K at 473 K, and the characteristic luminescence of Pr^{3+} is almost invisible. The phenomenon that the emission intensity of phosphors gradually decreases with the increase of temperature can be attributed to the thermal quenching effect. With the increase of temperature, the thermal energy obtained by the excited state ions increases, and the excited state energy is partially consumed by the thermal dissipation mechanism. The nonradiative relaxation process is enhanced, which reduces the probability of radiative transition, and resulting in reduced emission intensity.

Because 505 nm and 612 nm emission peaks come from different emission centers, they can not be directly used for FIR temperature measurement based on thermal coupling mechanism. However, the energy difference between the two emission peaks is moderate, and the peak positions do not overlap. Moreover, the emission intensity has an obvious strong and weak change with temperature, and the trend is clear. The FIR ratio decreases monotonously with temperature, which is suitable for fitting. Therefore, the 505 nm and 612 nm emission peaks can be used for FIR temperature measurement by using the non thermal coupling energy level strategy.

Fig.5 (c) shows the temperature dependence of the fluorescence intensity ratio (FIR) of the emission peaks of SNMV:0.03Pr^{3+} phosphor at 505 nm and 612 nm in the range of 98-298 K. It can be seen from the figure that the FIR value increases with the increase of temperature. The FIR of 505 nm and 612 nm are analyzed by cubic polynomial. The FIR can be expressed as[30-32]:

$$FIR = AT^3 + BT^2 + CT + D \quad (7)$$

Where T is the absolute temperature and A, B and C are relevant parameters. The results after fitting are shown in Fig.5 (c), from which we can see that all data points

View Article Online
DOI: 10.1039/D5DT02917A

are in good agreement with the fitting curve.

The absolute sensitivity (S_a) and relative sensitivity (S_r) of phosphors can be obtained from formulas 8 and 9:

$$S_a = |3Ax^2 + 2Bx + C| \tag{8}$$

$$\begin{aligned} Sr &= 100\% \times \left| \frac{1}{FIR} \bullet \frac{d(FIR)}{dT} \right| \\ &= 100\% \times \left| \frac{3Ax^2 + 2Bx + C}{Ax^3 + Bx^2 + Cx + D} \right| \end{aligned} \tag{9}$$

The parameters fitted in Fig.5 (c) are substituted into formula 8 and formula 9 to calculate the S_a value and S_r value within the range of 98-298 K, as shown in Fig.5 (d). The maximum S_a value and S_r value were 0.01782 K^{-1} (298 K) and 1.13543% K^{-1} (298 K), respectively.

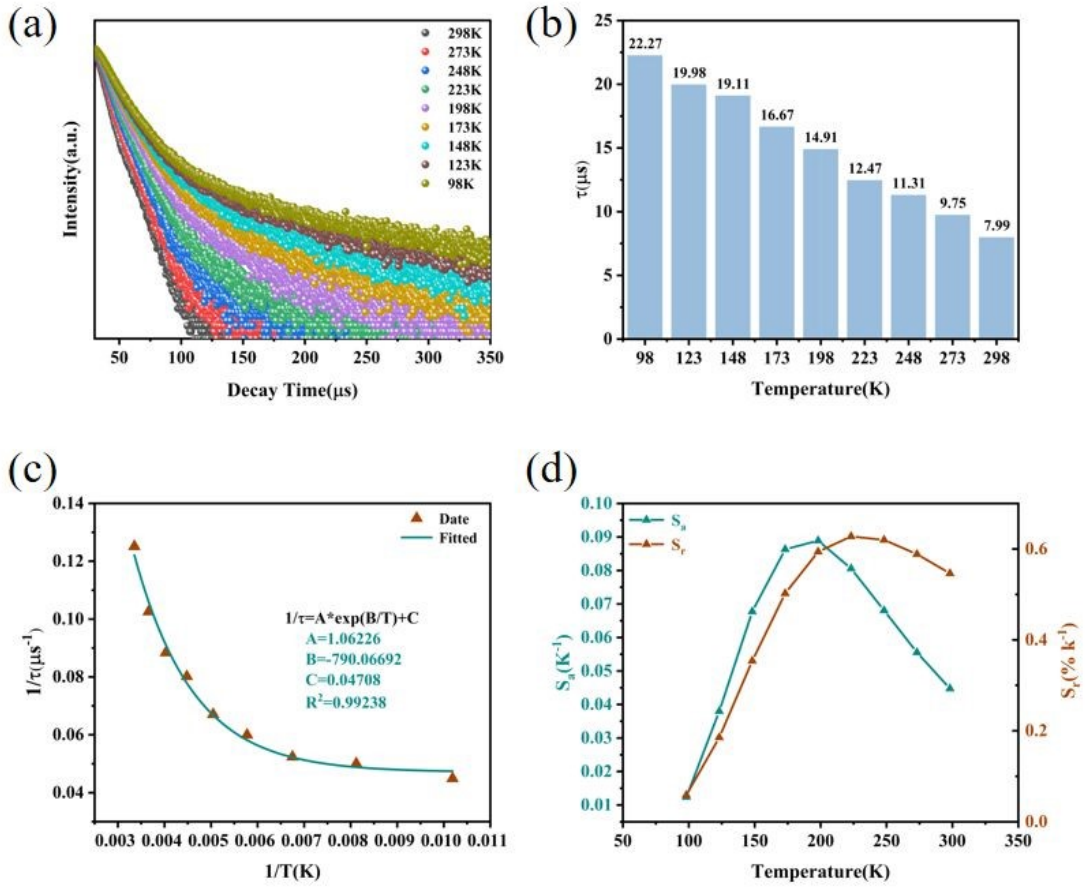

Fig.6 (a) Life decay curve of SNMV:0.03Pr^{3+} phosphor in the range of 98-298 K; (b) Comparison of fluorescence lifetime at different temperatures; (c) The temperature dependence of $1/\tau$ and $1/T$ of SNMV:0.03Pr^{3+} phosphor; (d) Absolute sensitivity S_a and relative sensitivity S_r versus temperature.

View Article Online
DOI: 10.1039/D5DT02917A

Fig.6 (a) shows the life decay curve of SNMV:0.03Pr^{3+} phosphor with temperature. It can be seen from the figure that the lifetime of phosphor gradually decreases with the increase of temperature. This is due to the increase in temperature, where the energy of the excited state is more dissipated through multi phonon assisted non radiative relaxation. This thermal quenching phenomenon not only reduces the luminescence efficiency, but also accelerates material aging, leading to a shortened lifespan of the phosphor. Fitting the life decay curve with the double exponential equation[33]:

$$I(t) = I_0 + A_1 \exp(\frac{t}{\tau_1}) + A_2 \exp(\frac{t}{\tau_2}) \quad (10)$$

Where I(t) is the luminous intensity at time t, τ_1 is the fast excited state lifetime, τ_2 is the slow excited state lifetime, and A_1 and A_2 are constants. The average decay life τ is calculated using formula11[34]:

$$\tau = \frac{A_1\tau_1^2 + A_2\tau_2^2}{A_1\tau_1 + A_2\tau_2} \quad (11)$$

As shown in Fig.6 (b), the average lifetime of phosphors decreases from 22.27 μs to 7.99 μs in the temperature range of 98-298 K. The relationship between $1/\tau$ and $1/T$ of phosphor is shown in Fig.6 (c). The Mottseitz model can be used to evaluate how temperature affects the fluorescence lifetime of samples[35].

$$\frac{\tau_0}{\tau(T)} = 1 + A\exp(\frac{-\Delta E}{K_B T}) \quad (12)$$

Where τ_0 is the life at 98 K, τ(T) is the life at a certain temperature, A is the fitting parameter related to non radiative transition, K_B is the Boltzmann constant, and ΔE is the thermal activation energy. Equation 12 can be further expanded as:

$$\frac{1}{\tau(T)} = B\exp(\frac{C}{T}) + D \quad (13)$$

Where B, C and D are parameters related to A and ΔE. The calculated values of B, C and D are 1.06226, -790.06692 and 0.04708, respectively. According to the function of phosphor decay life and temperature, the absolute sensitivity (S_a) and relative sensitivity (S_r) can be obtained from formulas 14 and 15:

$$S_a = \left|\frac{d\tau}{dT}\right| \quad (14)$$

View Article Online
DOI: 10.1039/D5DT02917A

$$S_r = 100\% \times \left| \frac{1}{\tau} \frac{d\tau}{dT} \right| \quad (15)$$

The parameters fitted in Fig.6 (c) are substituted into formulas 14 and 15 to calculate the S_a and S_r values within the temperature range of 98-298 K, as shown in Fig.6 (d). With the increase of temperature, S_a and S_r values first increased and then decreased, and the maximum S_a and S_r values were 0.0889 K^{-1} (198 K) and 0.62752% K^{-1} (223 K), respectively. Table 4 shows a comparison of temperature sensitivity characteristics within the low temperature range with reported materials[36-40]. It can be seen that SNMV: Pr^{3+} has relatively good optical temperature measurement performance.

Table 4 Temperature sensitivity comparison of reported phosphor**s**

Phosphors	Temperature (K)	Mode of thermometry	S_r (% K^{-1})	Ref.
$Sr_2InSbO_6:Cr^{3+}$	135-460	FL	0.73	36
$Lu_2Mg_2Al_2Si_2O_{12}:Bi^{3+}$, Tb^{3+},Eu^{3+}	98-498	FIR	0.21	37
$YbNbO_4:Er^{3+}$	120-280	FIR	0.712	38
$Sr_3MoO_6:Eu^{3+}/Tb^{3+}$	14-300	FIR	0.24	39
$Gd_2(MoO_4)_3$: Eu^{3+}, Tb^{3+}	80-450	FIR	0.5	40
$Sr_2NaMg_2V_3O_{12}:Pr^{3+}$	98-298	FIR	1.13543	This work
$Sr_2NaMg_2V_3O_{12}:Pr^{3+}$	98-298	FL	0.62752	This work

4. Conclusion

In this paper, SNMV:xPr^{3+} phosphor was synthesized by high temperature solid state method. The phosphor showed good temperature measurement performance at low temperature (98-298 K). Under the excitation of 339 nm, the phosphors exhibit strong blue-green broadband emission in the wavelength range of 400-700 nm and typical red narrow-band emission of Pr^{3+} at 612 nm and 624 nm, which correspond to the energy level transition of $[VO_4]^{3-}$ group and the $^1D_2 \rightarrow {}^3H_{4,5}$ transition of Pr^{3+}, respectively. The strongest emission peak of the host was near 505 nm, and the strongest characteristic emission peak of Pr^{3+} was at 612 nm. The change trend of the

View Article Online
DOI: 10.1039/D5DT02917A

intensity ratio of the two emission peaks at 505 nm and 612 nm with temperature was used for FIR optical temperature measurement. The maximum S_a and S_r values were 0.01782 K^{-1} (298 K) and 1.13543% K^{-1} (298 K), respectively. In addition, the average lifetime of phosphors decreases from 22.27 μs to 7.99 μs with the increase of temperature. FL optical temperature measurement was carried out based on the variation trend of fluorescence lifetime with temperature. The maximum S_a and S_r values were 0.0889 K^{-1} (198 K) and 0.62752% K^{-1} (223 K), respectively. To sum up, SNMV:xPr^{3+} phosphor has achieved high sensitivity dual-mode optical temperature measurement in low temperature region, showing a good application prospect in extreme environmental monitoring and other fields.

ASSOCIATED CONTENT

Notes

The authors declare no competing financial interests.

Acknowledgment

The research was financially supported by the National Key R&D program of China (Grant No. 2019YFA0709100), the National Natural Science Foundation of China (Grant No. 22175169).

References

[1] C.D.S. Brites, S. Balabhadra and L.D. Carlos, *Adv. Opt. Mater.*, 2019, **7**, 1801239.

[2] C. Tejas and S.D. Kamath, *ECS J. Solid State Sc.*, 2024, **13**, 077002.

[3] H. Suo, X. Q. Zhao, Z. Y. Zhang, Y. Wang, J. S. Sun, M. K. Jin and C. F. Guo, *Laser & Photonics Rev.*, 2021, **15**, 2000319.

[4] M. Fhoula, K. Saidi, C. Hernández-Álvarez, K. Soler-Carracedo, M. Dammak and I.R. Martín, *J. Alloys Compd.*, 2024, **979**, 173537.

[5] G. T. Xiang, Y. Y. Yi, Y. Zhang, M. Xiong, Q. Y. Xu, H. D. Chen, Y. Chang and L. Yao, *Chinese journal of luminescence*, 2024, **45**, 952-958.

[6] J. L. Fan, P. Sun, J. P. Gao, X. Cui, D. J. Fan, J. Cai, Y. Wen, J. M. Li and G. Wang, *J. Test Measur. Technol.*, 2025, **39**, 276-283.

[7] I. Kachou, K. Saidi, U. Ekim, M. Dammak, M. C. Ersundu and A. E. Ersundu, *Heliyon*, 2024, **10**, e30062.

[8] W. Liu, D. Zhao, R. J. Zhang, Q. X. Yao and S. Y. Zhu, *Inorg. Chem.*, 2022, **61**, 16468-16476.

[9] A. Siaï, P. Haro-González, K. Horchani Naifer and M. Férid, *Opt. Mater.*, 2018, **76**, 34-41.

[10] S. Gharouel, L. Labrador-Páez, P. Haro-González, K. Horchani-Naifer and M. Férid, *J. Lumin.*, 2018, **201**, 372-383.

[11] Y. Bahrouni, I. Kachou, K. Saidi, C. Hernández-Álvarez, M. Dammak and I. R. Martín, *J. Mater. Chem. C*, 2025, **13**, 13415-13425.

[12] Y. B. Yan, S. Li, S. S. Ding, B. X. Zhang, H. Sun, Q. H. Ju and L. Yao, *Acta Phys. Sin.*, 2024, **73**, 097801.

[13] A. Bindhu, J. I. Naseemabeevi and S. Ganesanpotti, *Dalton Trans.*, 2023, **52**, 11705-11715.

[14] J. K. Li, B. Liu, G. Y. Liu, Q. D. Che, Y. Z. Lu and Z. M. Liu, *J. Rare Earth.*, 2023, **41**, 1689-1695.

[15] A. Bindhu, J. I. Naseemabeevi and S. Ganesanpotti, *Adv. Photonics Res.*, 2022, **3**, 2100159.

[16] N. Navya, B. R. R. Krushna, S. C. Sharma, N. R. Nadar, M. Panda, A. George, C. Krithika, S. Rajeswari, R. Vanithamani, K. Madhavi, G. Ramakrishna, K. Manjunatha, S. Y. Wu and H. Nagabhushana, *J. Photochem. Photobiol. A: Chem.*, 2024, **456**, 115858.

[17] Anu and A. S. Rao, *Opt. Mater.*, 2023, **145**, 114476.

[18] J. J. Zheng, H. L. Shen, Y. F. Li, H. C. Li and Z. Yue, *J. Alloys Compd.*, 2023, **968**, 172112.

[19] W. Z. Lv, W. Lü, N. Guo, Y. C. Jia, Q. Zhao, M. M. Jiao, B. Q. Shao and H. P. You, *RSC Adv.*, 2013, **3**, 16034-16039.

[20] A.M. Pires and M.R. Davolos, *Chem. Mater.*, 2001, **13**, 21–27.

DOI: 10.1039/D5DT02917A

[21] S. Kumar, R. Prakash, V. Kumar, G. M. Bhalerao, R. J. Choudhary and D. M. Phase, *Adv. Powder Technol.*, 2015, **26**, 1263-1268.

[22] K. J. Albert , E. Muthulakshmi and S. M. M. Kennedy, *Mater. Sci. Eng. B*, 2026, **323**, 118737.

[23] H. T. Zhou, N. Guo, X. Lü, Y. Ding, L. Wang, R. Z. Ouyang and B. Q. Shao, *J. Lumin.*, 2020, **217**, 116758.

[24] X. Chen, Z. G. Xia, M. Yi, X. C. Wu and H. Xin, *J. Phys. Chem. Solids*, 2013, **74**, 1439-1443.

[25] L. X. Yang, X. Y. Mi, H. L. Zhang, X. Y. Zhang, Z. H. Bai and J. Lin, *J. Alloys Compd.*, 2019, **787**, 815-822.

[26] K. Li, D. Q. Chen, J. Xu, R. Zhang, Y. L. Yu and Y. S. Wang, *Mater. Res. Bull.*, 2014, **49**, 677-681.

[27] G. Blasse, *J. Solid State Chem.*, 1986, **62**, 207-211.

[28] K. Li, M. M. Shang, D. L. Geng, H. Z. Lian, Y. Zhang, J. Fan and J. Lin, *Inorg. Chem.*, 2014, **53**, 6743-6751.

[29] K. Li, M. M. Shang, H. Z. Lian and J. Lin, *Inorg. Chem.*, 2015, **54**, 7992-8002.

[30] V. K. Rai and S. B. Rai, *Appl. Phys. B*, 2007, **87**, 323-325.

[31]S. S. Zhou, G. C. Jiang, X. T. Wei, C. K. Duan, Y. H. Chen and M. Yin, *J. Nanosci. Nanotechnol.*, 2014, **14**, 3739-3742.

[32] Y. J. Wang, V. Tsiumra, Q. Peng, H. B. Liang, Y. Zhydachevskyy, M. Chaika, P. Dluzewski, H. Przybylinska and A. Suchocki, *J. Phys. Chem. A*, 2019, **123**, 4021-4033.

[33] K. E. Piecka, J. Drabik, D. Jaque and L. Marciniak, *Royal Society of Chemistry*, 2020, **22**, 25949-25962.

[34] X. Q. Xu, J. Ren, G. R. Chen, D. S. Kong, C. J. Gu, C. M. Chen and L. R. Kong, *Opt. Mater. Express*, 2013, **3**, 1727–1732.

[35] H. T. Zhou, N. Guo, M. M. Zhu, J. Li, Y. Q. Miao and B. Q. Shao, *J. Lumin.*, 2020, **224**, 117311.

[36] W. Zhao, L. Li, Z. J. Wu, Y. J. Wang, Z. M. Cao, F. L. Ling, S. Jiang, G. T. Xiang, X. J. Zhou and Y. B. Hua, *J. Alloys Compd.*, 2023, 965, 171370.

[37] Z. B. Zheng, Z. L. Li, Y. X. Zhao, Q. Y. Tao, L. Li, Y. H. Song, H. F. Zou and Z.

View Article Online
DOI: 10.1039/D5DT02917A

Shi, *J. Am. Ceram. Soc*., 2024, 107, 4064-4076.

[38] H. M. Ji, X. Z. Tang, H. Y. Zhang, X. L. Li and Y. N. Qian, *J. Coatings*, 2021, 11, 383.

[39] D.V.M. Paiva, S.K. Jakka, M.A.S. Silva, J.P.C. do Nascimento, M.P. F. Graça, A.S.B. Sombra, M.J. Soares, S.E. Mazzetto, P.B.A. Fechine and K. Pavani, *Optik*, 2021, 246, 167825.

[40] L. Han, J. Q. Liu, P. Liu, B. H. Li, X. L. Li and Y. Xu, *J. Phys. Chem. Solids*, 2021, 153, 110032.

View Article Online
DOI: 10.1039/D5DT02917A

Data Availability Statement

All data generated or analyzed during this study are included in this published article.